Magneto-convective effect on tritium transport at breeder unit level for the WCLL breeding blanket of DEMO

Magneto-convective effect on tritium transport at breeder unit level for the WCLL breeding blanket of DEMO

Ciro Alberghi[a], Luigi Candido[a], Raffaella Testoni[a], Marco Utili[b], Massimo Zucchetti[a]

[a]*Dipartimento Energia "Galileo Ferraris" – Politecnico di Torino, Corso Duca degli Abruzzi 24 – Torino (TO), Italy*
[b]*ENEA FSN-ING-QMN - C.R. Brasimone, Località Brasimone, Camugnano (BO), Italy*

The Water-Cooled Lithium-Lead (WCLL) is one of the four breeding blanket concepts proposed by Europe in view of its DEMO reactor. The velocity field of the electrically conducting lead-lithium eutectic alloy inside the blanket is strongly influenced by the external magnetic field used for plasma confinement combined with buoyancy effect. The strength of the magnetohydrodynamics (MHD) effect and of the magneto-convective effect (MHD and buoyancy force) depends on the intensity of the magnetic field and its orientation with respect to the direction of the lead-lithium motion. This phenomenon significantly influences the resulting temperature and velocity fields, and therefore the tritium transport inside the breeding blanket. A multi-physics approach of a 3D tritium transport model is presented for a simplified geometry of the WCLL breeding blanket. In particular, advection-diffusion of tritium into the lead-lithium eutectic alloy, transfer of tritium from the liquid interface towards the steel, diffusion of tritium inside the steel, transfer of tritium from the steel towards the coolant, and advection-diffusion of diatomic tritium into the coolant, temperature field, velocity fields of both lead-lithium and water, buoyancy forces, and MHD effect have been included in this study. The tritium concentrations and the inventories inside the lead-lithium, in the Eurofer pipes and in the baffle, and in the water coolant have been evaluated.

Keywords: WCLL, breeding blanket, DEMO, tritium transport, magneto-convection, MHD, buoyancy forces

1. Introduction

In a DEMO fusion reactor, the prediction of tritium concentrations and inventories in the blanket and the quantification of the permeation rate from the lead-lithium into the coolant is of main interest, both to guarantee fuel self-sufficiency and from a safety viewpoint [1]. Tritium represents a potential radiological risk [2], and, for this reason, its permeation towards the cooling system must be controlled to an acceptable level [3].

The multi-physics of the system, multi-material domains, and complex blanket geometry characterize some issues in the development of a tritium transport model. In literature, some tritium transport models can be found both at breeder unit level and at system level [4-8]; however, none of them takes into account also the impact of the magnetoconvective effect. Authors have also developed tritium transport models [3, 9-11] at breeder unit level for the Helium-Cooled Lithium-Lead (HCLL) and for the Water-Cooled Lithium-Lead (WCLL) breeding blanket, two of the four breeding blanket concepts proposed by Europe.

In this paper, a 3D tritium transport model for a simplified WCLL geometry has been carried out taking into account advection-diffusion of tritium into the lead-lithium eutectic alloy, transfer of tritium from the liquid interface towards the steel, diffusion of tritium inside the steel, transfer of tritium from the steel towards the coolant, and advection-diffusion of diatomic tritium into the coolant, temperature field, velocity fields of both lead-lithium and water. In particular, the combined effect of buoyancy forces and magnetohydrodynamics effect on tritium transport has been analyzed. In fact, the velocity field of the lead-lithium liquid metal is strongly influenced by the external magnetic field used to confine the plasma.

2. Description of the model

2.1 Reference geometry

In 2018, the WCLL geometry has been deeply changed [12]. In particular, the water tubes are arranged in a staggered way, hence it is not possible to identify an elementary cell as reference breeder unit as investigated in [10], but half a module has been identified as reference breeder unit. In Figure 1a, the reference breeder unit is shown. The Eurofer domain consists of water pipes, represented in green, and horizontal baffle plates, coloured in orange. The water and the lithium-lead domains are depicted in blue (Fig.1b) and grey, respectively.

It is important to notice that the horizontal stiffening plates and the first wall are not modelled in this work. The main geometry parameters are reported in Table 1. This reference geometry has been considered in the development of a CFD analysis.

(a)

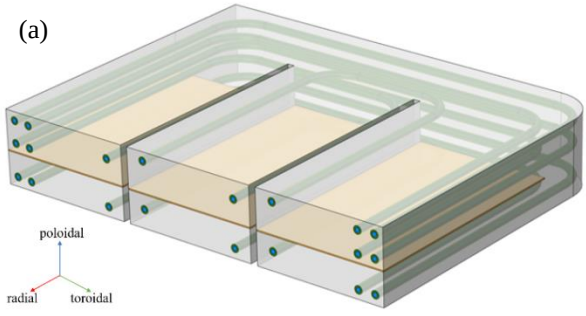

author's email: raffaella.testoni@polito.it

(b)

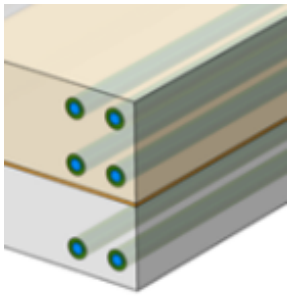

Fig. 1. (a) WCLL reference geometry for the breeder unit, (b) a zoom of the water tubes [12].

Due to the complexity of the geometry considered for the CFD model, a preliminary analysis of the MHD, and magneto-convective effect on the tritium transport has been performed with a simplified geometry that considers one-twelfth of the module including one coolant tube, as shown in Figure 2.

Table 1. Main geometrical parameters of the WCLL reference geometry.

Parameter	Description	Value [mm]
L_r	Radial length	540
L_p	Poloidal length	124
L_{tor}	Toroidal length	719
D_{ext}	Pipes external diameter	13.5
D_{int}	Pipes internal diameter	8
p_{baffle}	Toroidal pitch between the baffles	12
t_{baffle}	Baffle thickness	2
H_u	Height of PbLi channel, exit	66.5
H_d	Height of PbLi channel, inlet	55.5
R	Bending radius	9.375

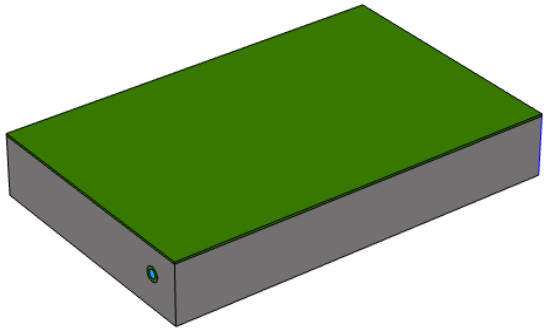

Fig. 2. Simplified WCLL reference geometry for the tritium transport model including MHD effect and buoyancy forces.

2.2 Solution techniques and governing equations

The numerical strategy to investigate the tritium transport, including the magneto-convective effect, has been developed as follows. First, the CFD model has been solved for the WCLL reference geometry for the breeder unit (Fig.1), considering buoyancy forces. The buoyancy effect has been implemented by using a gravity ramping technique [13]. This strategy has been adopted in order to mitigate the high non-linearity of the partial differential equations system due to the introduction of the volume force term. The CFD analysis has been carried out for two main reasons. Firstly, due to the new reference breeder unit respect to the previous studies [3, 10], the investigation of temperature and velocity field has been carried out in order to verify the correct set-up of the model. Secondly, this study represents the first step for the future implementation of tritium transport and magneto-convective effect at the reference the breeder unit level. As far as the general tritium transport investigation is concerned, a preliminary analysis has been carried out in a simplified geometry (Fig.2). In particular, the magnetic field effect has been introduced to evaluate the impact on tritium transport. Both the pure MHD and the magneto-convection effects have been solved. The modelling activity has been performed by means of COMSOL Multiphysics [13].

2.2.1 CFD governing equations

As a first step, the CFD analysis has been set-up. The buoyancy effect has been modelled under the Boussinesq hypothesis, for which the density variation has no effect on the flow field, except for the term which gives rise to the buoyancy force. The Navier-Stokes equation of continuity and momentum conservation can be written as follows:

$$\nabla \cdot \vec{u} = 0 \quad (1)$$

$$\rho_0(\vec{u} \cdot \nabla\vec{u}) = -\nabla p + \mu\nabla^2\vec{u} + k_{ramp} \cdot (\rho_0 + \Delta\rho)\vec{g} \quad (2)$$

where $\vec{u}$ [m·s^{-1}] is the velocity field, ρ_0 [kg·m^{-3}] is the reference density, p [Pa] is the pressure, μ [Pa·s] is the dynamic viscosity, k_{ramp} [-] is the ramping parameter and $\vec{g}$ [m·s^{-2}] is the gravity vector. In order to solve the velocity, pressure, temperature, and buoyancy fields, an iterative procedure has been implemented [10]. Eqs. (1-2) are simultaneously solved with the convective-conductive heat transfer equation:

$$\rho c_p \vec{u} \cdot \nabla T + \nabla \cdot (-k\nabla T) = \dot{Q} \quad (3)$$

where T [K] is the temperature, c_p [J·kg^{-1}·K^{-1}] is the specific heat at constant pressure, k [W·m^{-1}·K^{-1}] is the thermal conductivity and $\dot{Q}$ [W·m^{-3}] is the volumetric heat generation rate, that is space-dependent along the radial coordinate. The materials properties have been taken from [14]. The main input data implemented in the model are reported in Table 2.

Table 2. Main input data.

Data	Description	Value
$T_{in,LM}$	Lead-lithium inlet temp.	325 [°C]
p_{LM}	Lead-lithium inlet pressure	5 [bar]
v_{LM}	Lead-lithium inlet vel.	1 [mm·s^{-1}]
Φ_{ext}	FW thermal heat flux	0.5 [MW·m^{-2}]
Φ_{FW}	Thermal heat flux B.C.	$0.1 \cdot \Phi_{ext}$[MW·m^{-2}]
$T_{in,w}$	Water inlet temperature	285 [°C]
$v_{w,FW}$	Water inlet velocity in FW	1.24 [m·s^{-1}]

$v_{w,BZ}$	Water inlet velocity in BZ	1.57 [m·s^{-1}]
p_w	Water inlet pressure	155 [bar]

2.2.2 MHD governing equations

MHD studies the behaviour of liquid metals subjected to magnetic fields. Therefore, to describe the MHD governing equations, the Navier-Stokes equations must be modified considering the interaction between the conductive liquid metal and the applied magnetic field. In fusion blanket, the liquid metal is characterized by a Reynolds magnetic number $R_m \ll 1$. This means that the magnetic field can be considered as purely diffusive: any perturbation due to the fluid motion is smoothed out [15]. For a steady magnetic field and incompressible medium, the governing MHD equations under the low magnetic Reynolds approximation, in addition to continuity (1), and convective-conductive heat transfer equations (3), are:

$$\rho_0(\vec{u}\cdot\nabla\vec{u}) = -\nabla p + \mu_f\nabla^2\vec{u} + \vec{J}\times\vec{B} + (\rho_0 + \Delta\rho)\vec{g} \quad (4)$$

$$\nabla\cdot(\nabla\phi) = \nabla\cdot(\vec{u}\times\vec{B}) \quad (5)$$

where $\vec{J}$ [A·m^{-2}] is the current density, $\vec{B}$ [T] is the magnetic flux density, and ϕ [V] is the electric potential.

The two main fundamental parameters that influence MHD flow are the Hartmann number (Ha), and the wall conductance ratio (c_w). The Hartmann number, whose square represents the ratio of the Lorentz force to viscous forces, is expressed as:

$$Ha = B\cdot L\cdot\sqrt{\frac{\sigma_f}{\mu_f}} \quad (8)$$

where σ_f [S·m^{-1}] is the electric conductivity of the fluid, L [m] is a typical length-scale, Re [-] is the hydrodynamic Reynolds number. The wall conductance ratio is defined as follows:

$$c_w = \frac{\sigma_w\, t_w}{\sigma_f L} \quad (9)$$

where σ_w [S·m^{-1}] is the electrical conductivity of the wall and t_w [m] is the thickness of the wall. It assumes zero value in the case of electrically insulated walls, whereas it tends to infinity in the case of perfectly conducting walls. For the present calculations, σ_w=0.156 has been assumed for both the baffle and the pipes [12].

2.2.3 Tritium transport governing equations

A passive, scalar, general tritium transport equation can be written as follows:

$$\frac{\partial c_i}{\partial t} + (\nabla\cdot\vec{u})c_i + \nabla\cdot(-D_i\nabla c_i) = s_i \quad (10)$$

where c_i [mol·m^{-3}] is the tritium concentration in the i-th domain (lead-lithium, Eurofer, water), D_i [m^2·s^{-1}] is the diffusion coefficient of tritium and s_i [mol·m^{-3}·s^{-1}] is the molar tritium generation rate along the radial coordinate [3, 10].

As far as the main boundary conditions are concerned, the continuity of the pressure at lead-lithium/Eurofer interface has been imposed, and the flux continuity has to be guaranteed at the Eurofer/water interface. The detailed equations imposed as boundary conditions are reported in [10]. The tritium fluxes at the outlet of their corresponding domain (Pb-15.7Li outlet, water outlet) have been modelled assuming that the diffusion contribution is much smaller than the convective contribution [10]. Regarding the initial conditions, they have been set equal to zero at each domain.

3. Results

In this section, the main results are shown. First, the CFD analysis developed on the half a module (Fig.1) is presented. Then, the magnetohydrodynamics and magneto-convective effects on tritium transport model are shown in a simplified geometry (Fig. 2).

3.1 CFD analysis

3.1.1 Mesh and grid convergence

To ensure a minimum discretization error, a grid convergence study is performed, using the grid convergence index (GCI) method [16-18]. Three different grids are selected and are indicated as M1, M2 and M3, where M1 is the finest and M3 the coarser. The average-quality mesh M2 is reported in Figure 3, as an example. The mesh quality (skewness and condition number) and the total number of elements for all three selected meshes are reported in Table 3. In particular, the skewness is a measure of the asymmetry of the probability distribution of a real-valued random variable about its mean, whereas the condition number measures the distance of an element from the set of non-convex or inverted elements. Its optimization increases this distance and improves the shape quality of the elements.

Fig. 3. Mesh M2 for the full domain.

Table 3. Mesh quality and total number of elements.

	M1	M2	M3
Mesh quality measure (skewness)	0.7415	0.7283	0.7146
Mesh quality measure (condition number)	0.7551	0.63	0.5389
Total number of elements	1318879	528077	319725

The parameter that allows estimating the relative discretization error of the computed solution is the GCI. It has been estimated following the procedure reported in [16]. In particular, twenty local and global variables have been identified (represented by ID number reported in Figure 4), to evaluate the GCI. The results of the method

are shown in Figure 4. It can be stated that the coarser M3 mesh presents an average GCI, with respect to the M2, equal to 7.73%, whereas the M1 mesh presents an average GCI equal to 1.97%. Low values of GCI indicate the grid independence, and, for this work, a GCI smaller than 10% is assumed acceptable. Considering the results and the computational time needed to perform the calculations, the mesh M2 has been chosen as reference mesh.

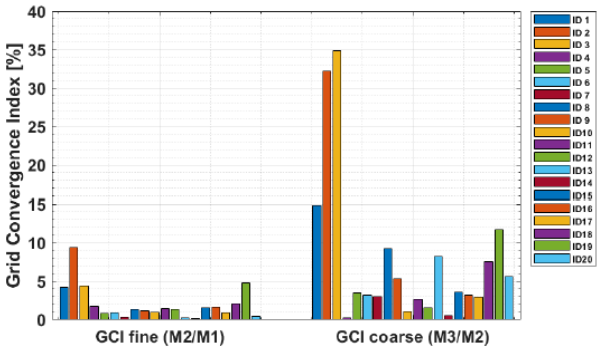

Fig. 4. Grid convergence index for the three different meshes. The legend represents the considered local and global variables.

3.1.2 CFD results

With reference to Figure 1, the Pb-15.7Li enters in the three rectangular ducts on the bottom of the module and exits from the three on the top. As boundary conditions, average velocity in the inlet and null pressure in the outlet are imposed. Water enters in the eight tubes on the left, removes the heat from the blanket and exits from the tubes on the right. BCs are equivalent to the ones for the Pb-15.7Li. The other conditions are no-slip in all the other boundaries. Heat transfer is solved considering adiabatic conditions in all the external surface excluded the boundaries facing the first wall, on which heat flux is imposed, that is a conservative assumption. This approach is useful to evaluate the impact of the buoyancies on the velocity and temperature profiles.

First, the no-buoyancy case is reported. In Figure 5, the Pb-15.7Li velocity field in the radial-poloidal plane placed in the middle of the module is presented. The arrows indicate the stream direction and are proportional to the velocity. The Pb-15.7Li flow is fully developed at the outlet of the sub-module. The average velocity is 0.78 $mm \cdot s^{-1}$, whereas the maximum is 2.37 $mm \cdot s^{-1}$ in the proximity of the baffle. In Figure 6, the temperature field is shown. The peak temperature is placed near the first wall, where the heat flux is incoming, and the volumetric heat generation rate is maximum. The maximum temperature in the Pb-15.7Li is 1367 °C, whereas in the Eurofer pipes and baffle is 808 °C, and 752°C, respectively.

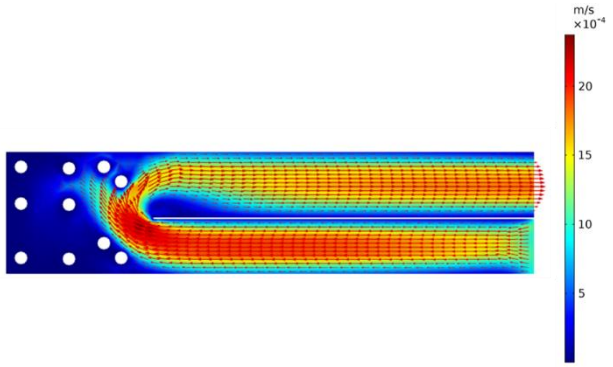

Fig. 5. Velocity profile for the case without buoyancy.

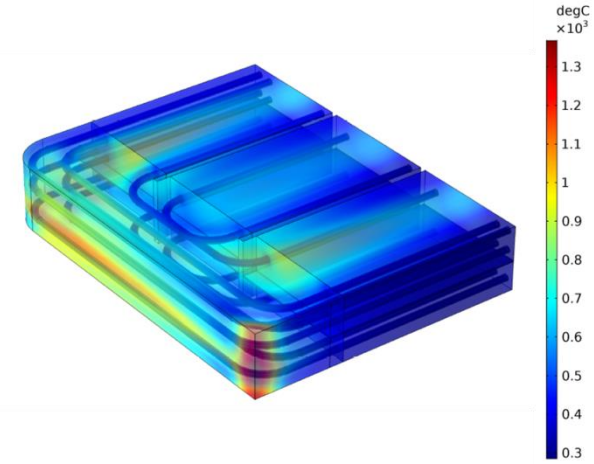

Fig. 6. Temperature profile for the case without buoyancy.

Then, the buoyancy case is reported. In Figure 7, the velocity profile is presented. A spot of high velocity near the exit can be seen, as well as an incoming flow from the outlet. This backflow phenomenon may be due to the low velocity of the Pb-15.7Li circulating in the blanket and to the dominant effect that buoyancy has on the flow behaviour, that can be seen comparing Figures 5 and 7. It may be also due to the boundary conditions adopted, and further investigations are needed, as explained below. In Figure 8, the temperature field is shown. The peak temperature is extremely smaller than in the no buoyancy case. The maximum temperature decreases up to 458 °C in Pb-15.7Li, whereas up to 431 °C in the Eurofer pipes and 372 °C in Eurofer baffle.

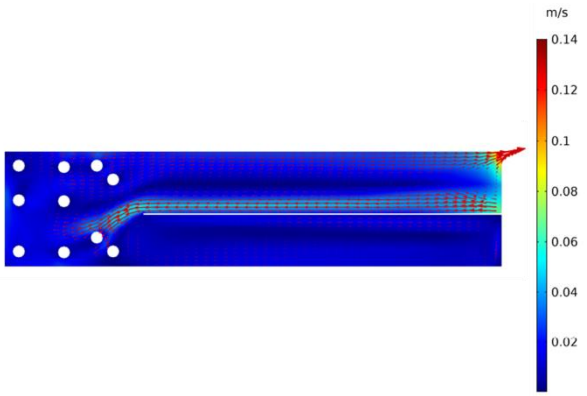

Fig. 7. Velocity profile for the case with buoyancy.

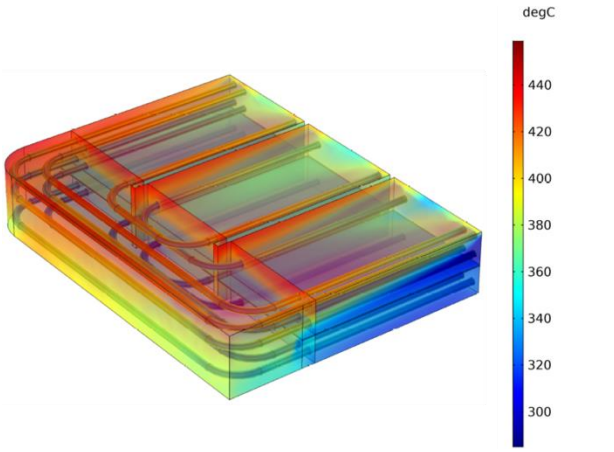

Fig. 8. Temperature profile for the case with buoyancy.

Comparing the two cases investigated, it is evident that buoyancy plays a major role, smoothing the temperature field, hence it cannot be neglected. Concerning the velocity field, the high thermal gradients tend to form vortexes and closed flow patterns inside the sub-module, causing backflow in the proximity of the outlet section. This creates a jet velocity with high peak values. In order to better understand this behaviour, as suggested in [16], a smaller outlet section should be considered. Thus, in future studies, the manifold should be included in the modelling, in order to verify if the outflow is a real problem or is a matter of computation domains used in the simulations.

3.2 Tritium transport analysis

In this section, the tritium transport models developed are reported for the simplified geometry reported in Figure 2. The magnetohydrodynamics effect has been also added and a preliminary analysis on its impact on tritium transport has been carried out. Both the pure MHD and the magneto-convection case have been solved for three different Hartmann number equal to 0, 5000, and 10000.

3.2.1 Velocity profile and permeation rate

In Figure 9, the Pb-15.7Li velocity profile in the poloidal direction (here labelled as z-direction) at the middle of the outlet section for different Ha numbers is shown, both for MHD and magneto-convection cases, respectively. The typical M-shape profile is present, but it is deformed by the presence of the tube. In the magneto-convection case, the velocity profile is changed by the effect of the gravitational term and it shifts towards the pipe. Velocity peaks of 0.14 $m \cdot s^{-1}$, $5.9 \cdot 10^{-3}$ $m \cdot s^{-1}$ and $3.27 \cdot 10^{-3}$ $m \cdot s^{-1}$ are reached in magneto-convection for $Ha = 0, 5000, 10000$, respectively, in comparison to $2.0 \cdot 10^{-3}$ $m \cdot s^{-1}$, $2.57 \cdot 10^{-3}$ $m \cdot s^{-1}$ and $3.1 \cdot 10^{-3}$ $m \cdot s^{-1}$ for the MHD case. This means that buoyancy forces tend to freeze the velocity field as Ha number increases. As in the CFD analysis, in the magneto-convection case, recirculation and backflow are present. Concerning the emperature field, the results are not reported here, but as expected and shown in the CFD analysis, the introduction of buoyancies tends to reduce and uniform temperatures. In Figure 10, the permeation rate, defined as the surface integral of the normal total flux on the interfaces between Pb-15.7Li and Eurofer, is reported as a function of the three different Ha number, for MHD and magneto-convection cases, respectively. It is possible to notice that it decreases as the Hartmann number increases in both cases. In the magneto-convection case, permeation rates are increased respect to the pure MHD, and they have a similar value for Ha=5000 and Ha=10000 due to the velocity profile that shows a similar behaviour (Fig 9b).

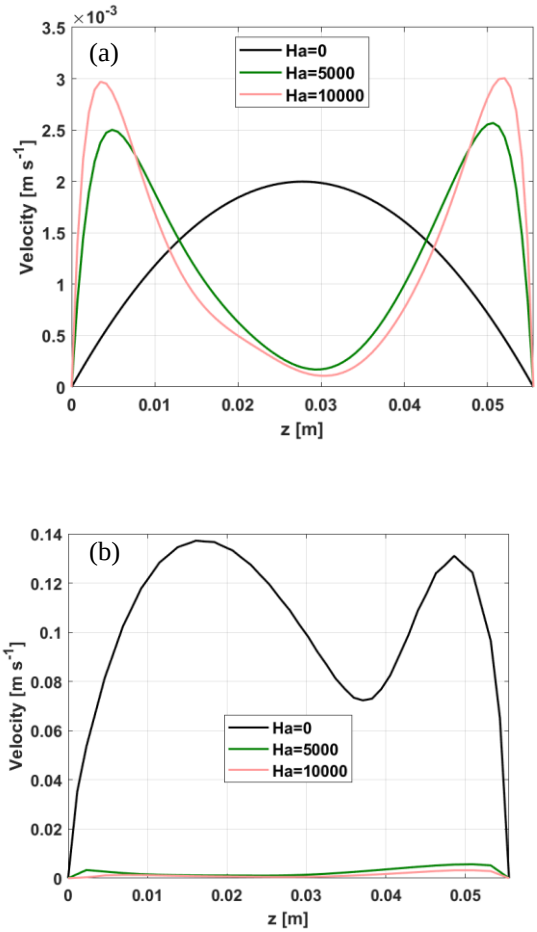

Fig. 9. Velocity on z-direction for different Ha at the outlet section, for MHD (a) and magneto-convection (b) case.

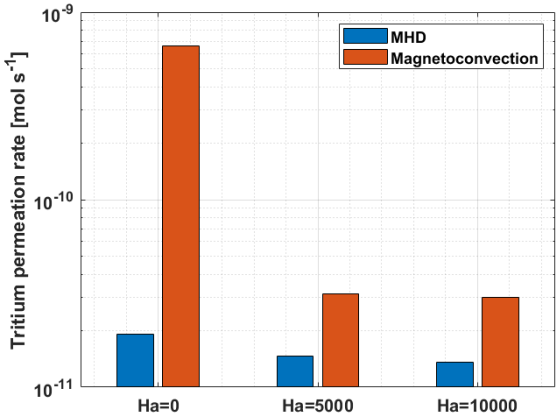

Fig. 10. Permeation rate as a function of the Hartmann number for the MHD and magneto-convection cases.

3.2.2 Comparison tritium transport for MHD and magneto-convection cases

In Figure 11, a 3D plot of tritium concentration in 5 slices along the radial direction is shown for the case Ha=10000, both for MHD case and magneto-convection case, respectively. The magneto-convection has a large effect on the flow behaviour, and as consequence on the tritium transport concentration profile. Due to the buoyancy forces, the temperature profile is more uniform, as expected. In addition, the magneto-convection produces backflow, and it tends to reduce the concentration of tritium in the domains. The estimation of tritium inventory in each domain has been carried out and it is reported in Table 4. It can be observed that the total inventory is similar in both MHD and magneto-convection cases, as expected.

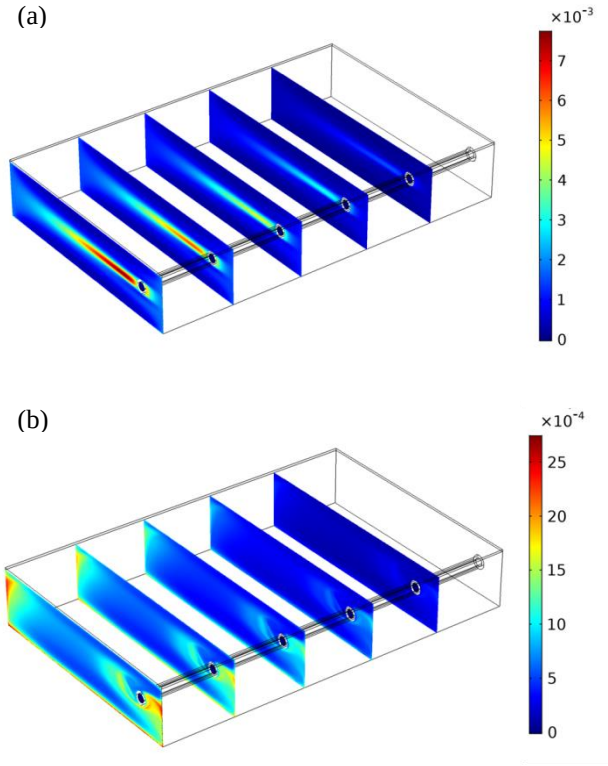

Fig. 11. Tritium concentration profile [mol·m^{-3}] for Ha=10000 and for MHD and magneto-convection cases, respectively.

Table 4. Tritium inventory for Ha=10000 for both MHD and magneto-convection cases.

	PbLi [μg]	Pipes [μg]	Baffle [μg]	Water [μg]	Tot [μg]
MHD	6.11	0.2	0.32	3.34E-5	6.63
Magneto-convection	5.94	0.07	0.42	1.24E-5	6.43

4. Conclusions

In this work, a CFD model of half-module has been performed comparing the case without buoyancy and with buoyancy forces. It has been observed that the introduction of the buoyancies tends to smooth the temperature field. Instead, for what concerns the velocity field, the high thermal gradients tend to form vortexes and closed flow patterns inside the sub-module, causing backflow in the proximity of the outlet section, an aspect which needs to be further investigated.

As far as tritium transport is concerned, a simplified geometry involving one-twelfth of the module has been considered with one tube. The velocity field of the Pb-15.7Li has been modelled taking into account the MHD effect and compared to the case in which also buoyancies are considered, i.e. the magneto-convective case. In the first case, the hydrodynamics profile is modified into the typical M-shape, with peak velocities increasing as Ha number increases. The permeation rate is reduced by 30% from Ha=0 to Ha=10000. In the magneto-convective case, the velocity profile is strongly decreased with respect to the case Ha=0, with peak velocities shifted in the toroidal direction and more asymmetric with respect to the previous case. The tritium permeation rate is about twice the one in the no-buoyancy case for the case Ha=5000 and Ha=10000. The highest permeation rate results in the Eurofer baffle, for which the inventory is 24% higher in the magneto-convective case respect to MHD; less tritium is retained in the Eurofer pipes, implying a lower inventory (about 1/3) in the water domain. The estimation of tritium inventories shows the conservation of the total amount in both cases.

The work needs to be deeply investigated in order to implement step by step the real geometry.

References

[1] S. Malang, et al., An example pathway to a fusion power plant system based on lead-lithium breeder: comparison of the dual-coolant lead-lithium (DCLL) blanket with the helium-cooled lead-lithium (HCLL) concept as initial step, Fusion Eng. Des. 84 (2009) 2145–2157.

[2] U. Fischer, et al., Neutronics requirements for a DEMO fusion power plant, Fusion Eng. Des. 98–99 (2015) 2134–2137.

[3] L. Candido, et al., Tritium transport in HCLL and WCLL DEMO blankets, Fusion Eng. Des. 109–111 (2016) 248–254.

[4] H. Zhang, et al., Quantification of dominating factors in tritium permeation in PbLi blankets, Fusion Sci. Technol. 68 (2015) 362–367.

[5] P. Zhao, et al., Tritium transport analysis for CFETR WCSB blanket, Fusion Eng. Des. 114 (2017) 26–32.

[6] L. Pan, et al., Tritium transport analysis of HCPB blanket for CFETR, Fusion Eng. Des. 113 (2016) 82–86.

[7] F. Urgorri, et al., Preliminary system modeling for the EUROfusion water cooled lithium lead blanket, Fusion Sci. Technol. 71 (2017) 444–449.

[8] E. Carella, et al., Tritium behavior in HCPB breeder blanket unit: modeling and experiments, Fusion Sci. Technol. 71 (3) (2017) 357–362.

[9] L. Candido, et al., Tritium transport model at the minimal functional unit level for HCLL and WCLL breeding blankets of DEMO, Fusion Eng. Des. 136 (2018) 1327–1331.

[10] L. Candido, et al., Tritium transport model at breeder unit

level for WCLL breeding blanket, Fusion Eng. Des. 146 (2019) 1207-1210.
[11] R. Testoni, at al., Tritium transport model at breeder unit level for HCLL breeding blanket, Fusion Eng. Des. (2019) https://doi.org/10.1016/j.fusengdes.2019.03.180 (in press)
[12] A. Del Nevo, et al., Recent progress in developing a feasible and integrated conceptual design of the WCLL BB in EUROfusion project, Fusion Eng. Des. (2019) https://doi.org/10.1016/j.fusengdes.2019.03.040 (in press)
[13] COMSOL Multiphysics. Available online: http://www.comsol.com/.
[14] D. Martelli, et al., Literature review of lead-lithium thermophysical properties, Fusion Eng. Des. 138 (2019) 183–195.
[15] P.A. Davidson. An introduction to Magnetohydrodynamics. Cambridge University Press, 2001.
[16] M. Casey and T. Wintergerste. Best practice guidelines. ERCOFTAC, 2000.
[17] I. Celik. Numerical uncertainty in fluid flow calculations: needs for future research. J Fluid Eng ASME, 115 (1993) 194-195.
[18] P. J. Roache et al., Editorial policy statement on the control of numerical accuracy. J Fluid Eng ASME, 108 (1986) 2.